Measurement 195 (2022) 111122

Contents lists available at ScienceDirect

Measurement

journal homepage: www.elsevier.com/locate/measurement

Exploiting phase-based motion magnification for the measurement of subtle 3D deformation maps with FP + 2D-DIC

L. Felipe-Sesé [a,*], A.J. Molina-Viedma [a], M. Pastor-Cintas [a], E. López-Alba [b], F.A. Díaz [b]

[a] Departamento de Ingeniería Mecánica y Minera, Campus Científico Tecnológico de Linares, Universidad de Jaén, 23700 Linares, Spain
[b] Departamento de Ingeniería Mecánica y Minera, Campus Las Lagunillas, Universidad de Jaén, 23071 Jaén, Spain

ARTICLE INFO

Keywords:
Phase-Based Motion Magnification
Digital Image correlation
Fringe Projection
Vibration analysis

ABSTRACT

Phase-Based Motion Magnification (PBMM) is an effective methodology to visualise imperceptible phenomena based on magnifying periodic subtle movements on image sequences. Moreover, the integration of the optical techniques Fringe Projection and 2D Digital Image Correlation (FP + 2D-DIC) make it possible to obtain 3D displacement maps employing a single camera.

In this study, the integration of PBMM with FP + 2D-DIC is exploited for the determination of subtle 3D displacements. An initial solid-rigid test validates of the combination of those techniques. A later test, employing a cantilever beam, demonstrates its correct performing in the determining of Operational Deflection Shapes. In both cases, the results are compared with those obtained with 3D-DIC and Scanning Laser Doppler Vibrometer (SLDV) to evaluate the relation between the magnification factor and the result obtained. Finally, the potential of the proposed integration for the determination of complex mode shapes is demonstrated by obtaining the ODSs of an industrial component.

1. Introduction

Full-field techniques have become popular in last decades for monitoring and determining the behaviour of components in machines and structures. Thanks to continuous development in digital cameras and processing software, they present several advantages compare to traditional pointwise measurement methods. Among others, it highlights the possibility to perform non-contact measurements and high spatial resolution data fields, which make it easier the interpretation of the behaviour. With the development of high-speed cameras, vibration analysis is one of the disciplines most benefited from these optical techniques. In fact, Digital Image Correlation (DIC) [1] has become widely employed in vibration analysis in researching field. It offers an interesting balance between accuracy, ease of operation and versatility [2,3]. In fact, several previous works have exploited it for modal analysis [4–7].

Compared to 2D-DIC, the early version of the technique, which employs a single camera for in-plane displacement, the 3D variant requires using two cameras [1]. It might represent a limitation in some situations and was the motivation of the development of the alternative treated in this work based on the integration of Fringe Projection (FP) [8–12] and 2D-DIC. The former is based on analysing the phase variation of a fringe pattern obliquely projected over a specimen to measure out-of-plane shape. The latter relies on tracking the speckle pattern sprayed on the specimen to obtain in-plane displacements maps. Both speckle and fringe patterns should be present on each captured image when employing FP + 2D-DIC in dynamic tests. This is possible employing RGB colour pattern encoding as usually employed in previous studies [13]. Thus, red speckle and blue fringe pattern can be separated employing a RGB camera and processed independently. This integration, named as FP + 2D-DIC, was proposed specially for dynamic events when high speed is required such in impact [14] or vibration analysis [15,16].

Both DIC and FP are based on the measurement of displacements and their accuracy is substantially based on the resolution of the cameras [1], among other set-up factors [17–19]. When employing high-speed cameras, resolution is usually lower than for low-frame rate cameras due to technical limitations related to the storage speed. In vibration analysis, that could represent a certain limitation especially when slight displacement occurs, for instance at high frequencies or when amplitude is reduced. In addition, although FP + 2D-DIC has been stablished as an interesting alternative to 3D-DIC, practical results show that

* Corresponding author.
E-mail address: lfelipe@ujaen.es (L. Felipe-Sesé).

https://doi.org/10.1016/j.measurement.2022.111122
Received 24 January 2022; Received in revised form 11 March 2022; Accepted 29 March 2022
Available online 1 April 2022
0263-2241/© 2022 The Author(s). Published by Elsevier Ltd. This is an open access article under the CC BY-NC-ND license (http://creativecommons.org/licenses/by-nc-nd/4.0/).

displacement contours tend to be nosier due to crosstalking between colour patterns [20], which could lead to additional issues in the achievement of mode shapes or operational deflection shapes [16].

Nonetheless, a recent methodology that allows the magnification of subtle periodic motion registered in an image sequence could improve those concerns. This methodology is Phase-Based Motion Magnification (PBMM) and consists in decomposing the registered frame sequence through complex steerable pyramid filters and magnifying an specific frequency band [21] by a magnification factor. This motion magnification was presented for a wide variety of applications related to revealing of invisible periodic phenomena, thanks to the capability to extract visual information from apparently steady sequences [22,23]. In fact, due to its high potential, the magnification tool was originally employed by the authors together with Digital Image Correlation for the characterisation of operational deflection shapes in two and three dimensions, obtaining information out of noisy maps [24–26]. In these studies, the displacement amplitude with the magnification factor trend was found to be linear. However, the actual factor did not correspond with the theoretically established.

That combination constitutes an interesting tool to understand the mechanical behaviour through the superimposition of displacement maps over magnified images. Other research works also follow a similar line and have employed PBMM together with different tracking frameworks. For instance, with particle tracking velocimetry (PTV) for the obtaining of modal information, both in 2D and 3D [27]. Additionally, PBMM present high potential in Health Monitoring as demonstrated by Civera et al. [28]. They demonstrated the possibility of detecting different damages on a cantilever specimen by analysing sequences of images of the specimen vibrating and applying PBMM and evaluating differences in ODS and frequency between original and damaged states. Eitner et al. [29] also demonstrated that, by magnifying the motion in a broad frequency band which contains all the active modes, the motion extraction with a point tracking algorithm can be greatly enhanced which lead to more accurate modal parameters.

From a different perspective, some authors propose employing the phase information directly to identify specific modal components without video magnification purposes. This line was firstly proposed by Yang et al. [30] who performed a methodology to estimate the full-field dynamic parameters of the deformation modes of a structure, as well as its rigid-body motion. Rohe et al. [31] also applied this approach noting that the extracted phases are proportional to displacements in the image. However, the results of this procedure are purely a shape expressed as phases instead of a motion magnitude, which could eventually complicate the interpretation of results, especially for 3D motion.

Despite the recent advances and uses of PBMM, using 3D-DIC to measure in magnified images is the only methodology to achieve 3D measurements in a full-field manner. The present work aims to alternative propose FP + 2D-DIC together with PBMM to obtain contours 3D displacement plots when subtle periodic deformations occur. As the measurement is a combination of FP and 2D-DIC techniques, PBMM must be independently applied to the image sets of each technique. In this study, the coherence between in- and out-of-plane displacements is thoroughly checked for a proper integration of measurements. For this purpose, the experimental campaign was designed to assess key points for the validity of the combination with motion magnification.

In the first case, the validation of the proposed approach is analysed through a rigid body displacement test. It is considered of main interest to verify that displacement maps during deformation are not distorted during magnification by comparing with well-established techniques such 3D-DIC.In the second one, the methodology is validated for operational deflection shapes measurements with a cantilever beam specimen. In both tests, 3D-DIC was employed to validate the results. Moreover, a quantitative evaluation of the relation between the magnification factor and the measured displacement is explored. Scanning Laser Doppler Vibrometry (SLDV), with a high sensitivity over vision techniques [5], was employed as a reference measurement. Finally, a test on a large industrial component employing high-speed cameras demonstrates the enhancement of the FP + 2D-DIC results with PBMM in the determination of contour of complex mode shapes in 3D surfaces and the potential of the proposed work.

2. Background

2.1. Phase-based motion magnification

Phase-based motion magnification is a new Eulerian approach to motion processing developed by Wadhwa et al. [21] to reveal subtle motion in videos by obtaining a magnified version. The video signal are decomposed using complex steerable pyramid filters [32]. This is an overcomplete transform based on complex sinusoids modulated by a Gaussian window function. Local amplitudes and phase were obtained according to spatial scale, orientation, and position.

The algorithm employs the phase signals of the complex steerable pyramids to identify the local motions in spatial sub-bands of an image. Previous studies [33,34] demonstrate that phase is more robust than amplitude defining the motion field reducing contrast and scale changes. The concept is analogous to Fourier shift theorem for sine functions transforms. The displacement term is encoded in the phase of each spatial frequency component. Thus, the time-domain local phase at every spatial scale and orientation of a steerable pyramid can be temporally bandpass filtered to isolate specific temporal frequencies relevant to a given application and remove any temporal DC component. This frequency band is then manipulated by multiplying by magnification factor, α. Analogously to Fourier shift theorem, the original phase can be modified by the amplified bandpassed phases which involves a magnification of the harmonic motion in the sequence corresponding to this frequency band after reconstructing the images. Therefore, a modified version of the video with that band eventually magnified by $(1 + \alpha)$ can be obtained by transforming the phase signal back to the time-domain and recomposing the images from the pyramids filters. In this process, an amplitude-weighted spatial smoothing is also applied to increase the signal-to-noise ratio.

2.2. FP + 2D-DIc

This combination of techniques was initially proposed as an economical alternative to 3D-DIC for 3D displacement measurements by simplifying and reducing the stereoscopic setup, composed of two cameras, to a single one. It is conceptually based on the complementarity of the measuring process and results of both techniques. Fringe projection (FP) is based on projecting parallel fringes on the specimen surface to determine the out-of-plane shape changes. This fringe pattern should be obliquely projected which lead to exhibit an in-plane displacement when the specimen experiences 3D displacement. The difference in phase of that projected fringes of the specimen during deformation with respect to a reference is analysed to extract a continuous map of out-of-plane displacements or shape. 2D-DIC [35] is light-intensity-based and relying on the use of digital image processing. In this technique, areas of recorded images are divided into virtual sets of pixels called facets that are tracked in subsequent images when displacement occurs. By determining the pixel translation of each facet relative to a reference image and using a proper calibration, the in-plane displacements are obtained. To perform a successful tracking, the specimen surface should present a randomly distributed speckle pattern to guarantee the singularity of each facet.

Hence, for the integration of FP and 2D-DIC, it is employed a conventional colour LCD projector and a colour RGB camera. The projector is employed to create a blue sinusoidal fringe pattern on white background. That permits fringe projection analysis to be performed in the blue spectrum of the recorded images to achieve out-of-plane displacements in z- direction [36,37]. In addition, a red speckle pattern on a white background is painted onto the measured surface to permit 2D-

DIC [38] to be performed in the red spectrum and measure in-plane displacements in x- and y- directions.

Additionally, the FP + 2D DIC integration must take into account that the in-plane displacements measured by 2D-DIC present a distortion when out–plane displacement or shape occur [13,37]. This effect is rectified using FP data with a mathematical correction methodology based on a pin-hole model of lenses which requires an specific calibration [13,39,40].

In the scope of this work, the image sequences obtained for each technique have to be magnified independently for each pattern but using the same parameters. Therefore, it is crucial to evaluate that fringe and speckle patterns experience the same magnification to ensure an accurate performance of the in-plane correction and, eventually, of the measurement. Fig. 1 present a flowchart of the procedure to obtain magnified 3D displacement maps from each of the RGB images.

3. Rigid body motion test

In the first test, the objective was to evaluate the accuracy of the integration focusing on the correction of the in-plane displacements after magnifying. A simple flat specimen was sinusoidally excited at a frequency quite below its resonances to produce a rigid body periodic translation without deformation. Namely, a plate of dimensions 100 × 400 × 7 mm was excited at 14 Hz employing a shaker DataPhysics GW-V20 in the out-of-plane direction, as shown in Fig. 2. The position of the plate along time represent parallel planes perpendicular to the optical axis, i.e., each of them represents pure out-of-plane displacement. These displacement maps are very appropriate to verify the correction process as stipulated in [39] and reveal any issue after magnification and its cause, reducing variabilities introduced by any deformation.

The FP + 2D-DIC system consisted of an EPSON EB-W32 projector and a 3CCD colour camera (JAI-AT-200GE, 16 mm lens, 1624x1236 pixel), as shown in Fig. 2. A blue fringe pattern of 2 pixels was projected to be employed for FP out-of-plane measurements, whereas a red speckle pattern was sprayed over a white background on the specimen surface for in-plane measurements with 2D-DIC. After separating the patterns using colour encoding, fringe pattern images were processed employing Fourier transform profilometry [8] and Quality Guided Unwrapping [41]. On the other hand, the speckle images were processed using a commercial DIC algorithm (VIC 2D by Correlated Solutions Inc.) using a facet size of 19 pixels and spacing of 5 pixels. The calibration was performed following a stipulated procedure [39,40], by which 11 images were captured from a distance of −1.5 mm to 1.5 mm with respect to the reference distance $z_0 = 720$ mm. The lateral magnification of the optical system was 0.20 px/mm.

A simultaneous measurement with a 3D-DIC system was also performed to compare the results with a 3D optical technique that has been already validated in combination with motion magnification [25]. This system, also shown in Fig. 2, consisted in two cameras (Alvium 12 Mpx 1800 U-1236c from Allied Vision) with 12 mm focal length lenses, obtaining a lateral magnification of 4.79 px/mm, close to FP + 2D-DIC camera, 4.73 px/mm. The speckle images were processed using a commercial DIC algorithm (VIC 3D by Correlated Solutions Inc.) using a facet size of 75 pixels and spacing of 20 pixels.

During the test, the recording followed a subsampling strategy. Both vision systems were synchronised, using a pulse train generated by a DAQ device NI 6211 to capture images at the specified frequency. A sequence of 188 images were captured at a frame rate of 4.7 fps. It ensured that entire cycles of the motion at 14 Hz were recorded at the alias frequency 0.1 Hz, yielding 47 images per cycle. The criteria to define the shutter exposure time was about ten times shorter than the period of the excitation in order to avoid any blurring. Thus, shutter was set to 1/140 s. Then, the images were magnified in a narrow band around the alias frequency.

Simultaneously but not synchronised, a SLDV, model PSV 400 by Polytec, was employed as a reference measurement to evaluate the magnification factor measured with the vision techniques. The scanning was performed in a mesh of 9 × 11 equidistant measurement points distributed in a squared region of interest. The measurement was executed on the back of the sample for simplicity in the set up. For illustrative purpose, the region of interest of each technique is shown in Fig. 3.

3.1. Results

In this rigid body test, which consisted in a low vibration, the motion amplitude was large enough to be detected by FP + 2D-DIC and 3D-DIC without magnifying. This allows to check the measurement in the original, non-magnified images with the SLDV. In Fig. 4 (a) it is presented the mean value of the out-of-plane displacement map measured with each technique. The time evolution in a harmonic shape can be observed corresponding to the applied sinusoidal excitation for both vision techniques, which were synchronised. As for the SLDV, measurement was simultaneous but not synchronised so the range of its signal is shown instead. Despite the low frequency vibration, a soft excitation was applied to have certain level of noise, as observed in the signals. Although, the capabilities of FP + 2D-DIC has been assessed in comparison with 3D-DIC in specific studies [13,39], this test shows that

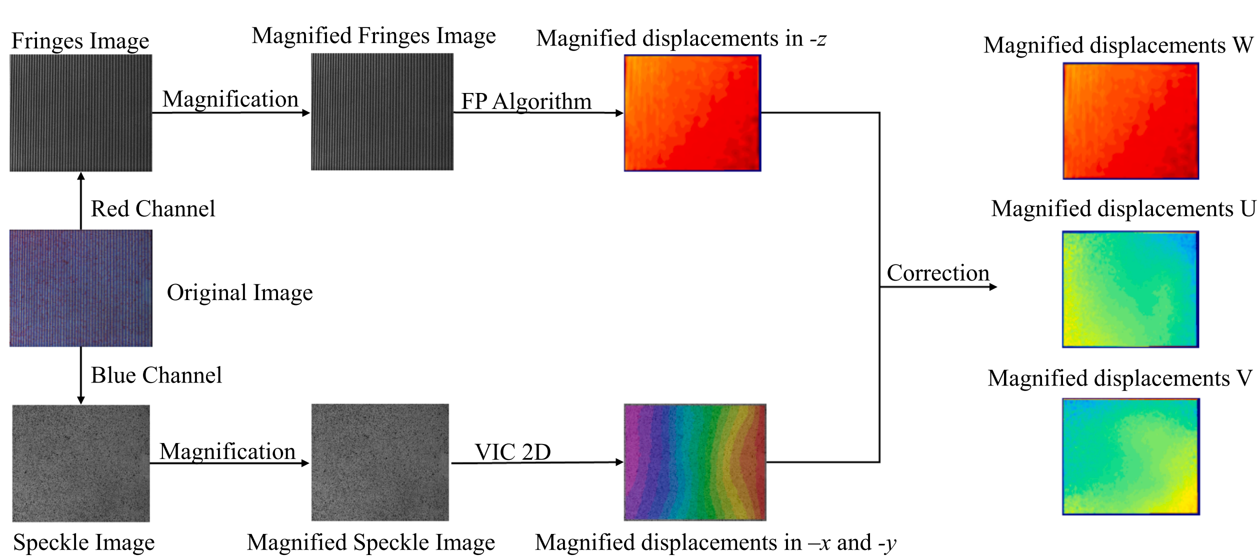

Fig. 1. Flowchart for obtaining 3D displacement maps using PBMM and FP + 2D-DIC.

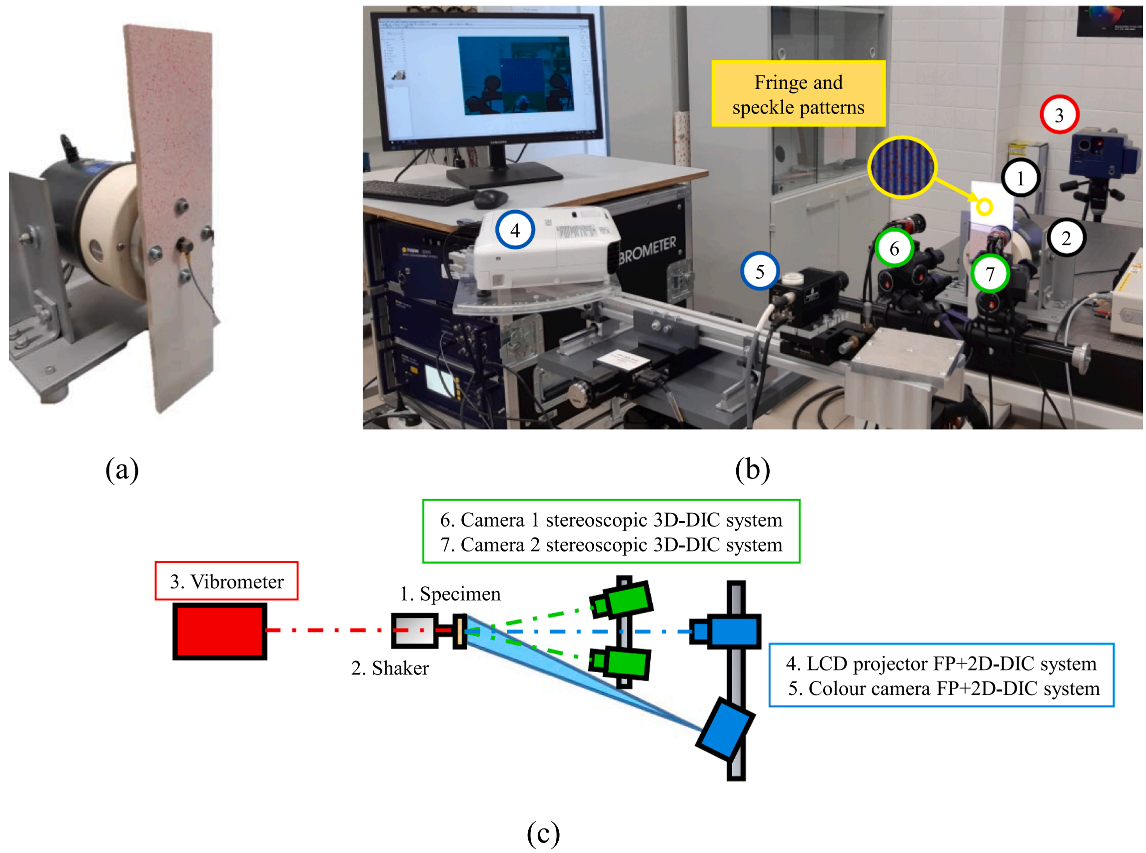

Fig. 2. Setup for the evaluation of in-plane displacement correction in FP + DIC: (a) Specimen mounted on the shaker's armature. (b) Picture and (c) scheme of the optical setups for FP + DIC, 3D-DIC systems and SLDV.

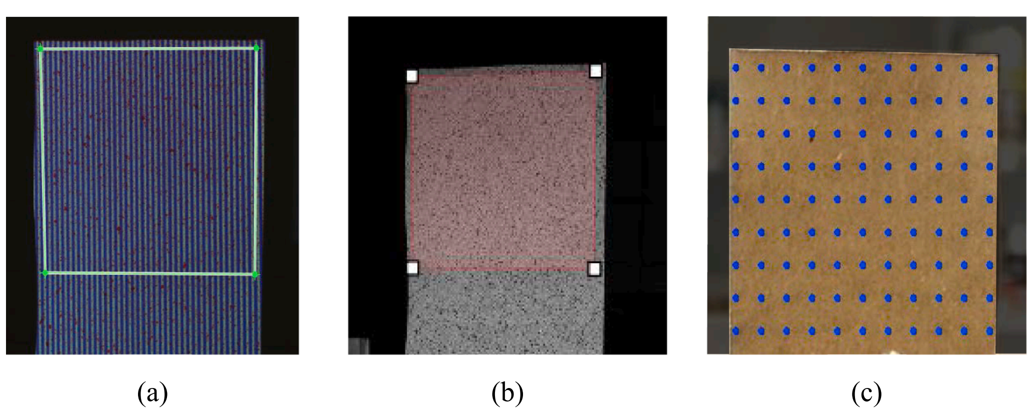

Fig. 3. Region of interest for each technique: (a) FP + 2D-DIC, (b) 3D-DIC and (c) SLDV.

it can provide measurement as accurate as 3D-DIC with a single camera, and both agree with the SLDV. The high sensitivity measurement of the latter yielded a 0.001 mm standard deviation of the amplitude in the measurement grid. This confirms the rigid behaviour of the plate.

However, the individual processing of fringe and speckle images for magnification requires new assessments. Three magnification factors were applied to the images: 5x, 10x and 15x. The plots in Fig. 5 show the displacement maps in the horizontal, U, and vertical, V, directions for the original non-magnified measurement, (a)-(b), and for 15x magnification, (c)-(d). As a rigid motion in the out-of-plane direction, the effect of the distortion of the in-plane motion is clearly seen as an inclination in the maps that represent a fictitious elongation of the plate. However, these maps must be constant. The mathematical correction of those distorted displacement maps proposed by Felipe-Sesé et al. [13] for the integration of FP + 2D-DIC, as commented in section 2.2, was able to subtract this effect After correction, U and V maps became practically constant. Analogous results were obtained for 5x and 10x factors. It shows that FP + 2D-DIC is suitable to be employed with magnified sequences of images. Fig. 4 (b) shows the mean out-of-plane displacement of the plate measured by FP + 2D-DIC. Magnification reduces the level of noise in the signal, as in previous studies with 3D-DIC [25]. However, this behaviour is better illustrated by the next tests.

4. Operational deflection shapes in flat plates

The second test aimed to evaluate the capabilities of the measurement with FP + 2D-DIC in magnified images for deformation in specimens. An operational deflection shape of a 2 mm thick polycarbonate

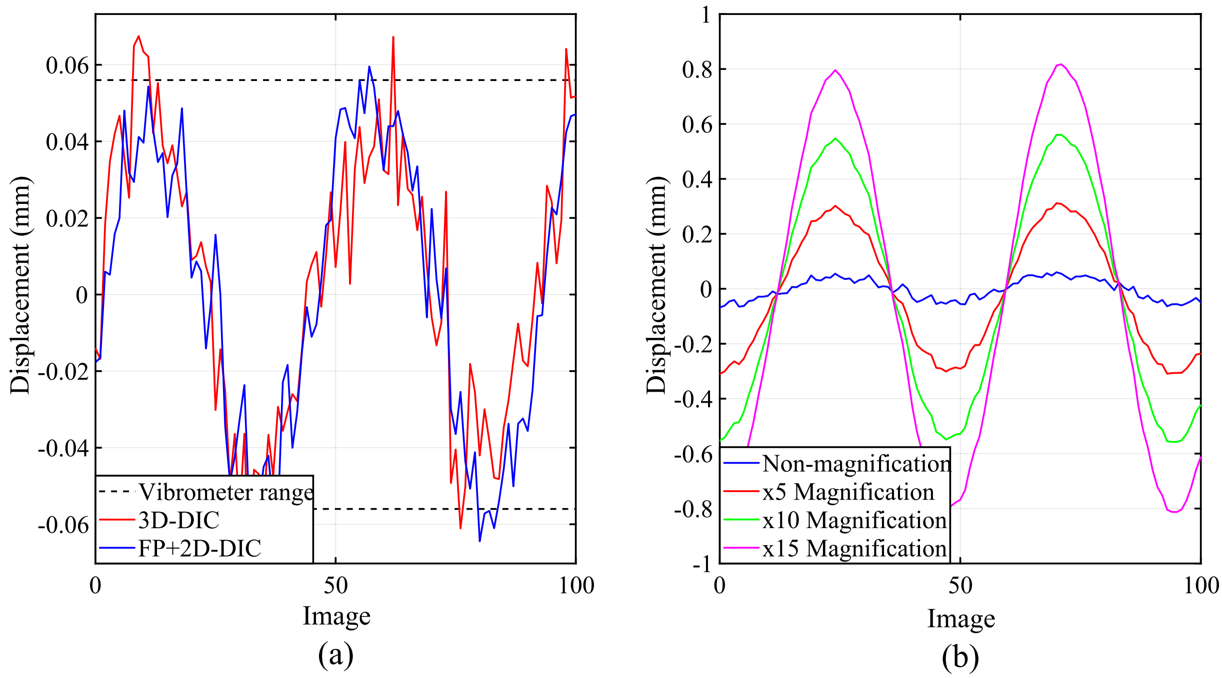

Fig. 4. Time histories of the mean out-of-plane rigid-body displacement of the plate: (a) Original sequence. (b) FP + 2D-DIC displacements in magnified sequences.

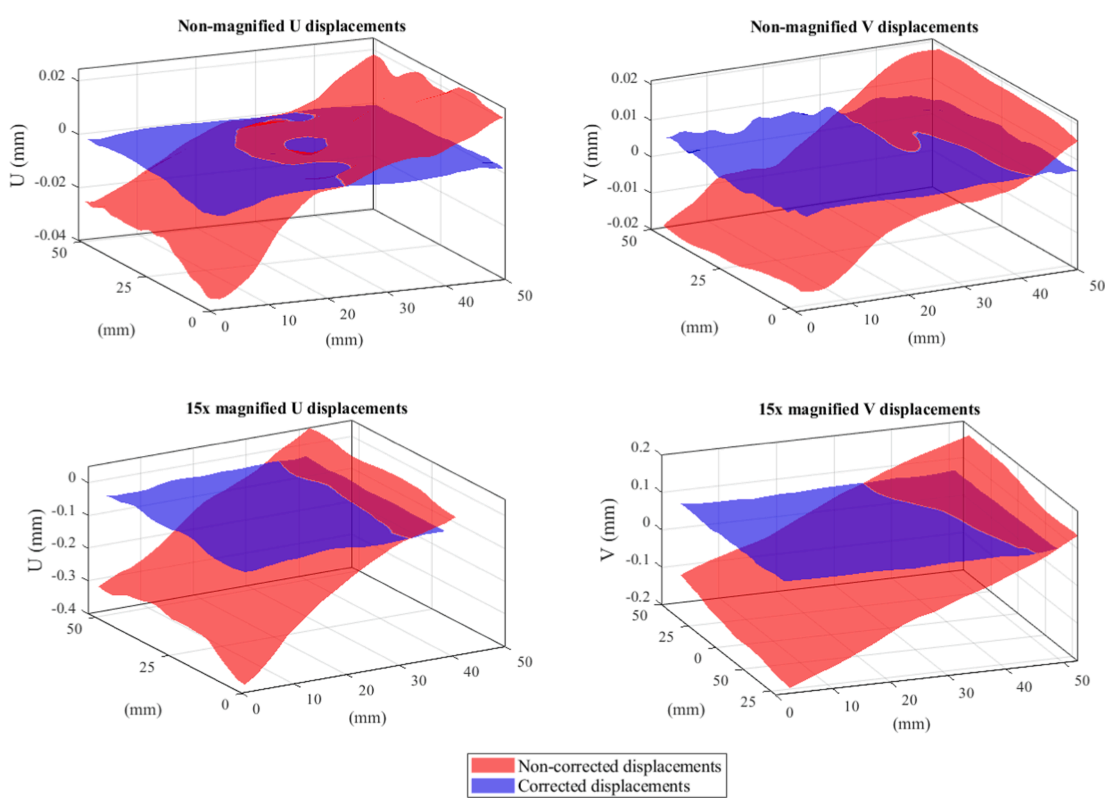

Fig. 5. Corrected and non-corrected in-plane displacements (horizontal, *U*, and vertical, *V*) of the rigid plate obtained from the original non-magnified sequence and the 15x magnified sequences.

plate, employed as a cantilever beam, was studied. The plate was harmonically excited at one resonance frequency using the shaker by attaching through a clamping device. As a result, the vibrating surface was 160 mm long and 40 mm wide. Again, the results were compared and validated through 3D-DIC measurements. Finally, the amplitudes obtained with both methods and its evolution with the magnification factor were assessed with the high-sensitivity measurement of the ODS using SLDV.

The natural frequencies of the beam were initially determined by means of a modal test employing the SLDV and an accelerometer placed on the clamping device. The shaker was provided with a white noise random signal up to 4000 Hz to build the transmissibility function between the response of the beam and the excitation of the shaker. From this result, the resonances of the specimen could be identified in the analysed spectrum.

For the selection of the frequency for this test, a middle order resonance was considered that shows the benefits of motion magnification for low signal-to-noise ratio maps. The low-frequency deflection shapes present high displacements, which are appreciable by the technique with a high signal-to-noise ratio and magnification is not required. On the other hand, the high-order ones are so low in amplitude that no information can be extracted even from the magnified image. Therefore, the third bending mode (475 Hz) was found to be the most illustrative for the purposes of this test.

The equipment employed was the same as the first test. The experimental setup for both vision measurements was hence similar. However, the vibrometer had to be placed in front of the beam in this occasion due to the laser beam interference with the shaker's body, losing a region of the specimen. Therefore, measurements with FP + 2D-DIC and 3D-DIC could not be performed at the same time due to the spatial restriction for the whole equipment. Each measurement was performed sequentially maintaining the same test conditions. The arrangement of each optical systems is shown in Fig. 6.

The recording was also performed under the considerations of the first test. 176 images were captured. To reduce the size of the sequences, the images resolution was cropped to fit the specimen shape, using 1380x440 pixels for FP + DIC and 2750 × 800 for 3D-DIC. The frame rate was established at 4.4 fps, with 22 images per cycle and 0.2 Hz alias frequency. Magnification of this frequency was applied to the images in a narrow band. The shutter was set to 1/4750 s. As for the SLDV, a grid of 105 points was scanned on the plate surface.

4.1. Results

In the previous test, it has been checked that the correction of in-plane displacements is properly performed from magnified images through an illustrative rigid body motion. Now, the combination is evaluated for specimens under periodical deformation. Specifically, the Operational Deflection Shape (ODS) of the cantilever beam at its resonance frequency of 475 Hz corresponding to its third bending mode under three magnification factors: 2, 5 and 10.

In Fig. 7, the measurement of the ODS using FP + 2D-DIC yielded a displacement maps in which no coherent bending deflection is observed. As magnification is applied in increasing factors, the maps corresponding to the third bending mode of a cantilever beam is revealed, with a progressive noise reduction. This behaviour was certified in previous studies for 3D-DIC, which serves here as validation results. The comparison of the different magnification states reveals similar shapes with both techniques. As a common feature, FP + 2D-DIC yields noisier maps as it might appear some crosstalk between fringe and speckle patterns and it gives a measurement point per pixel, while the maps of 3D-DIC are smoothed by the use of facets of several pixels. Beyond the shape validation, it is remarkable the difference of the magnitudes for the same magnification factor, which is discussed in the next section.

5. Evaluation of the linear trend of amplitude with magnification factor

According to [21], the chosen band of the phase signal during PBMM is magnified by $(1 + \alpha)$. This give a proportional evolution of the motion amplitude with the magnification factor. This section aims to evaluate this trend through the displacement measured with the vision techniques. In a previous study on 2D-DIC [24], this trend was found to be proportional but not following a factor of $(1 + \alpha)$.

The analysis of amplitudes in both previous tests also showed a deviation from this ideal. The actual magnification factor was estimated by comparing with the original amplitudes measured by SLDV. In the rigid body motion test, the mean displacement of the plate was employed for this purpose. For the bending deformation of the cantilever beam, the resulting magnification was calculated at every SLDV scanning point locations and, then, the mean value was obtained. It was necessary to match the grid location of the three techniques by considering a common reference, namely, one of the corners of the beam.

The result is shown in Fig. 8 for rigid body motion and ODS on flat specimen tests. The measured versus the computationally applied magnification factor is shown for every case. A linear fit was performed which confirmed the linear trend in all the cases. However, a deviation from the ideal line corresponding to a measured factor equal to $(1 + \alpha)$ is observed, depicted in a black dashed line. In both tests, FP + 2D-DIC obtained the closest values to the ideal trend as its fitting lines have the slope and offset parameter closest to one. The deviation of 3D-DIC could be significant. This implies that the amplitudes using one or another vision technique differ despite using the same magnification factor. This does not imply, though, a distortion of the real deformation, as demonstrated in previous studies [24,25]. Hence, it is not an obstacle for the characterisation of ODS, which are usually amplitude normalised.

Although out of the purpose of this study, the fact that the obtained magnification in FP + 2D-DIC is closer to the ideal might be consequence of the measurement principle for out-of-plane displacements. FP amplifies them through the in-plane motion of fringes, while 3D-DIC perform the out-of-plane measurement from the projection of this direction in the plane of each camera, which are usually almost perpendicular. PBMM detects and magnifies pixel-to-pixel (in-plane) motions of the different features in the images and, therefore, fringes motion is more detectable. Nevertheless, this point deserves a further study.

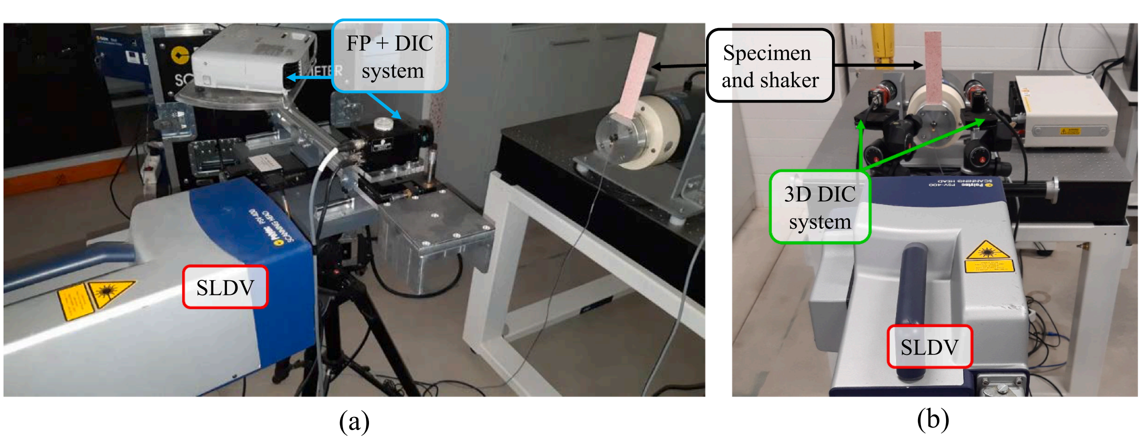

Fig. 6. Experimental setups for the ODSs measurement in the cantilever beam: (a) FP + DIC and (b) 3D-DIC.

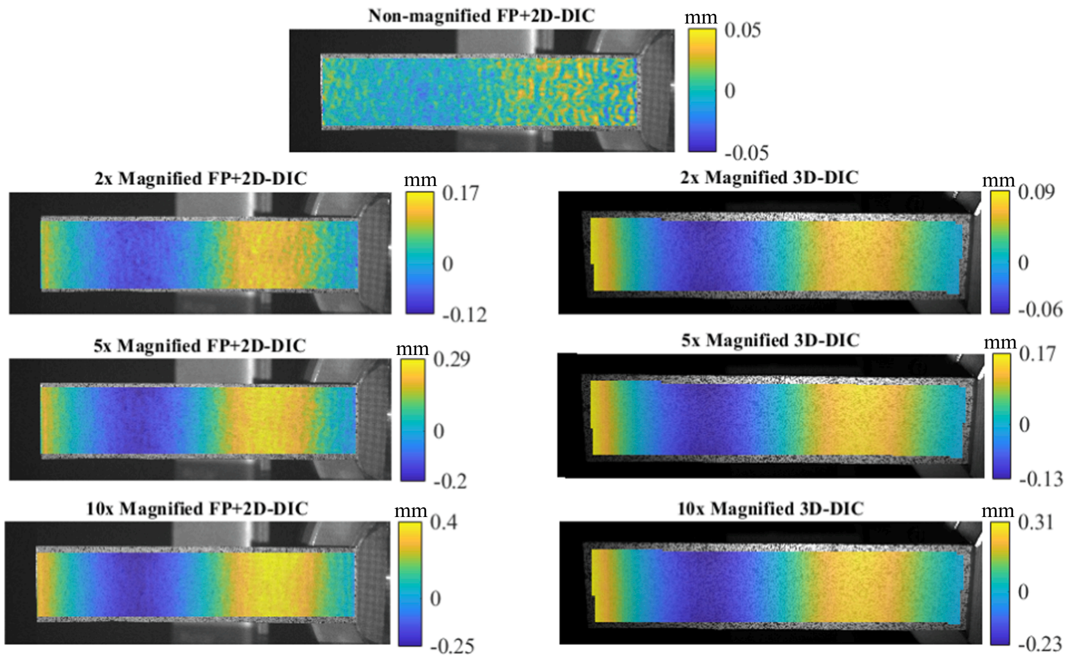

Fig. 7. Out-of-plane displacement maps (mm) of the third bending mode of the cantilever beam under different magnification factors using FP + 2D–DIC and 3D-DIC.

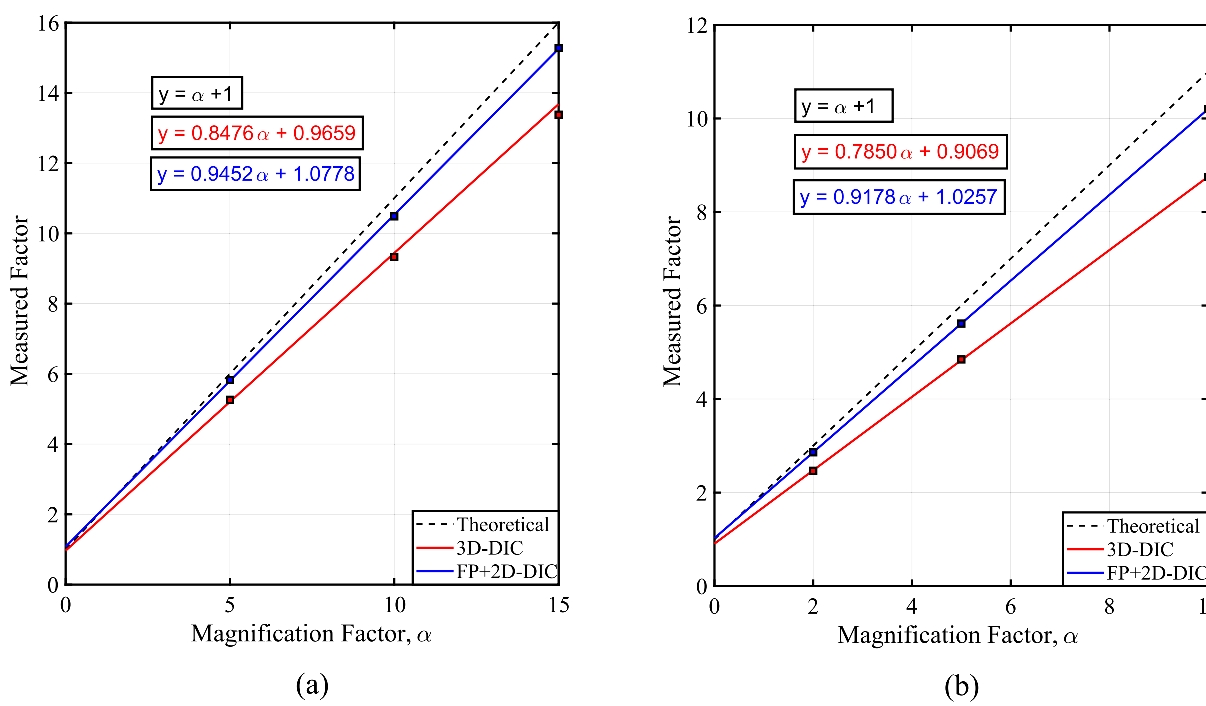

Fig. 8. Linear regression for measured magnification factors.(a) Results for rigid body motion tests (b) Results for ODS on flat specimen test.

6. Operational deflection shapes in industrial component

The purpose of this final test is to show the potential of the methodology to measure 3D ODSs in non-flat industrial components. A large-dimensions curved composite panel (1.45 m high, 2.0 m wide and 0.6 m deep) was hung from a frame structure to measure different ODSs at resonance frequencies under free-free boundary conditions. The panel was excited with the same shaker of previous tests using a stinger at a point in the middle of the lower edge. A resonances identification was initially performed up to 125 Hz, measuring the excitation applied by the stinger with a load cell and accelerometers for the panel response.

Afterwards, the panel was harmonically excited at each resonance for the optical measurement. The system consisted of the same projector and a single colour high-speed camera model SA3 (1 Mpixel) by Photron with a Vivitar lens (28 mm focal length). Patterns for FP and 2D-DIC was similarly employed. Considering the symmetry of geometry and load, half the panel was measured. This setup is shown in Fig. 9 [16,42]. Two resonances were tested. The first one was 47 Hz and was recorded at 500 fps in a 500 images long sequence. The second one was 74 Hz, recording 500 images at 1000 fps. Analogously, Fourier profilometry was

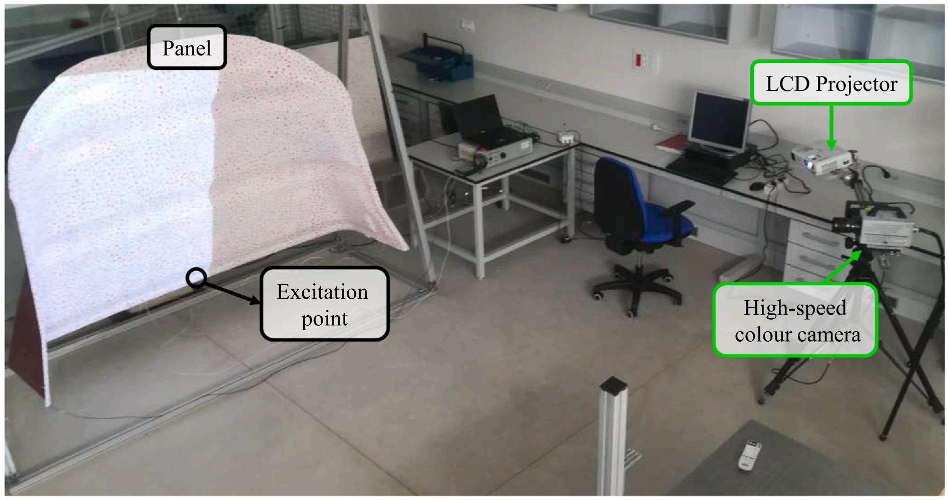

Fig. 9. Experimental setup for the ODSs measurement in the industrial panel using FP + 2D-DIC.

employed to process fringes motion, and 2D-DIC using facets of size 19 pixels and step 5 pixels.

6.1. Results

The ODSs at two of the resonance frequencies of the curved industrial panel were obtained using FP + 2D-DIC after magnifying the image sequence of the tests. These shapes are shown in Figs. 10 and 11, normalised by amplitude, and compared with the maps in the original images at the same instant. Due to the shape and deformation behaviour of the panel, the three orthogonal components of displacement are required: horizontal, U, vertical, V, and depthwise, W. The flexibility of the panel at these low frequencies is significant, even though, the original measurements are significantly polluted by noise and the shapes are not clear. The combination of FP + 2D-DIC and motion magnification reduced the presence of spatial noise and, thus, improved the quality of the ODSs maps.

The capability to give 3D displacements is a significant advantage of

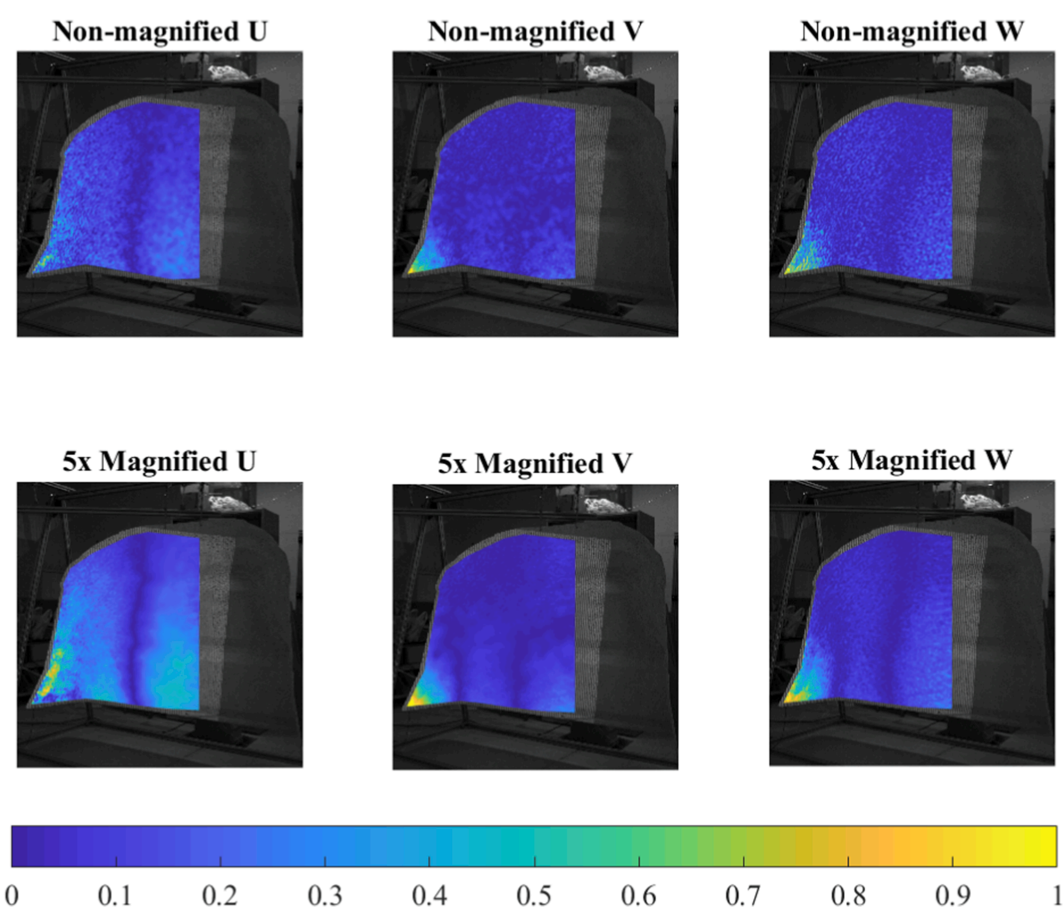

Fig. 10. Industrial panel 3D ODS at the 47 Hz resonance obtained by FP + DIC in the magnified and non-magnified sequence. Directions are: U, horizontal, V, vertical and W, depthwise.

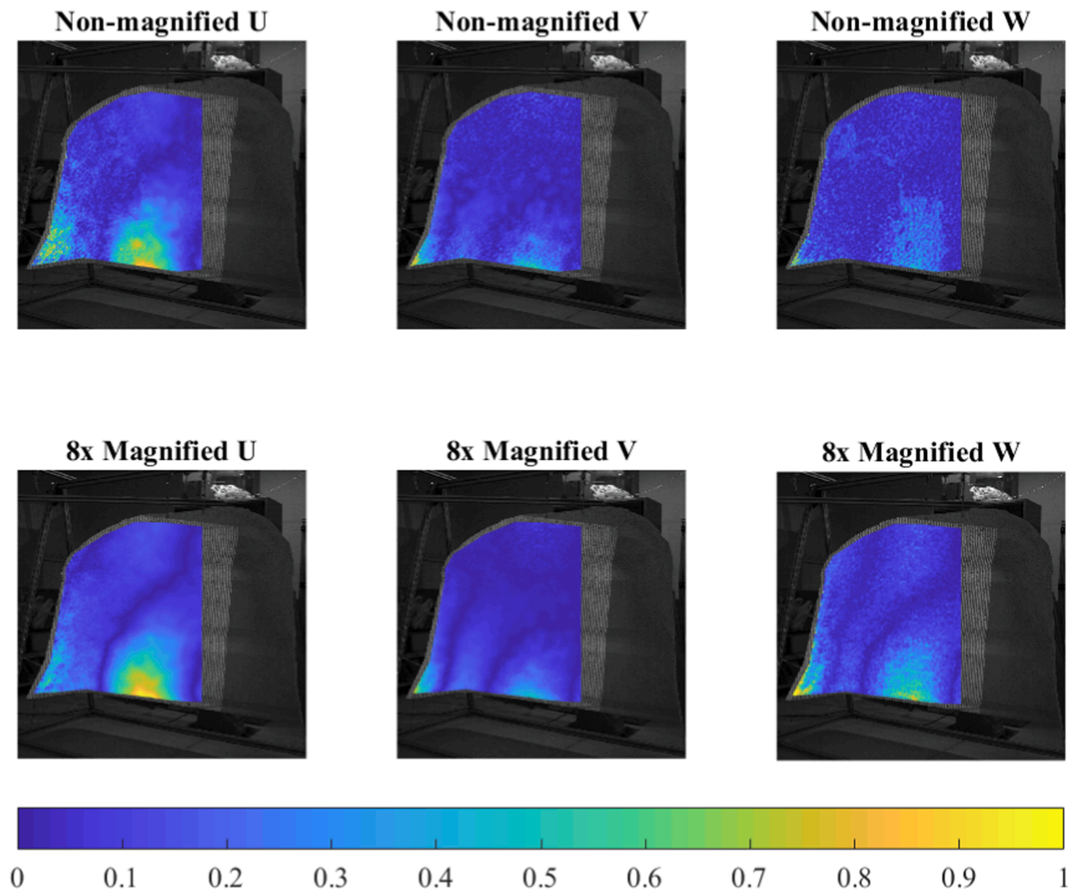

Fig. 11. Industrial panel 3D ODS at the 74 Hz resonance obtained by FP + DIC in the magnified and non-magnified sequence. Directions are: U, horizontal, V, vertical and W, depthwise.

these techniques over other applications of PBMM that are simply based on optical flow. This is especially relevant for this kind of curved plates. Additionally, FP + 2D-DIC performs with a unique camera. The visualisation of the motion with the maps overlaid provides a useful tool for the analysis of deforming structures in space, including simultaneous qualitative and quantitative information. To illustrate this, videos of the normalized ODSs at 47 and 74 Hz, magnified ×5 and ×8 respectively are provided as supplementary material.

7. Conclusions

This study has exploited the integration of Fringe Projection and 2D Digital Image Correlation for the determination of subtle periodic 3D displacement in combination with video motion magnification, using a single camera. This has been done through a deep evaluation of the intrinsic processing of FP + 2D-DIC integration and the results, in comparison with consolidated techniques. Namely, as this technique performs FP and 2D-DIC processing in simultaneous but different image sequences, both must be magnified individually.

First, the evaluation of the in-plane displacement correction was performed through the measurement of the rigid body motion of a flat plate. The pin-hole model correction was able to remove the spurious in-plane deformation yielding constant displacement maps, in spite of individually magnifying the sequences for FP and 2D-DIC.

In the next step, the combination of FP + 2D-DIC and PBMM was performed for the characterisation of ODSs in flat components. The evaluation of the measurement of the third bending mode of a cantilever beam revealed the agreement of the deformation maps of FP + 2D-DIC with those of 3D-DIC for the same magnification processing. In previous studies, the combination of 3D-DIC was proved to provide deflection shapes without any distortion introduced by magnification, therefore, this allows to validate FP DIC with PBMM for periodic deformation measurement.

In both test, the proportionality of the displacements with the magnification factor was analysed. Both for FP-DIC and 3D-DIC, proportionality was observed but it does not follow the trend defined by PBMM algorithms. It was found out that the relation between the expected magnification values were closer in the case of FP + 2D-DIC. This difference could rely on the fact that out-of-plane motion produces an amplified motion of the fringes, which might make it more suitable to be magnified by PBMM. However, this could be a line to explore in future investigations.

The high potential of the combination was demonstrated for the determination of 3D ODS in non-flat industrial components. Unlike other uses of PBMM, measuring on magnified images using FP + 2D-DIC, or 3D-DIC, is the only way to obtain 3D measurement maps to date. It is very beneficial for the interpretation of the behaviour of complex components under vibration.

Concluding, this investigation has expanded the application range of the optical technique FP + 2D-DIC. The displacement maps obtained by this technique, which aims to propose a simpler alternative to 3D-DIC, were usually nosier than those obtained by 3D-DIC. However, Phase-Based Motion Magnification, enhance the signal to noise ratio which could overcome that issue in experiments based on vibration or periodic excitation.

CRediT authorship contribution statement

L. Felipe-Sesé: Investigation, Conceptualization, Methodology, Data curation, Visualization, Writing – review & editing, Funding acquisition, Supervision. **A.J. Molina-Viedma:** Investigation, Conceptualization, Methodology, Software, Data curation, Visualization, Writing – review & editing. **M. Pastor-Cintas:** Investigation, Software, Data curation, Visualization, Writing – original draft. **E. López-Alba:** Investigation, Conceptualization, Methodology, Funding acquisition, Validation. **F.A. Díaz:** Supervision, Resources, Writing – review & editing.

Declaration of Competing Interest

The authors declare that they have no known competing financial interests or personal relationships that could have appeared to influence the work reported in this paper.

Acknowledgements

The authors gratefully acknowledge the financial support from the University of Jaén and Andalusian Government through the research project "Programa Operativo FEDER 2014-2020". Ref. 1263076 ", without which this work could not have been performed.

Appendix A. Supplementary material

Supplementary data to this article can be found online at https://doi.org/10.1016/j.measurement.2022.111122.

References

[1] H. Schreier, J.-J. Orteu, M.A. Sutton, Image Correlation for Shape, Motion and Deformation Measurements, Springer US, Boston, MA, MA, 2009. 10.1007/978-0-387-78747-3.
[2] M.N. Helfrick, C. Niezrecki, P. Avitabile, T. Schmidt, 3D digital image correlation methods for full-field vibration measurement, Mech. Syst. Signal Process. 25 (2011) 917–927, https://doi.org/10.1016/j.ymssp.2010.08.013.
[3] T.J. Beberniss, D.A. Ehrhardt, High-speed 3D digital image correlation vibration measurement: Recent advancements and noted limitations, Mech. Syst. Signal Process. 86 (2017) 35–48, https://doi.org/10.1016/j.ymssp.2016.04.014.
[4] Á.J. Molina-Viedma, E. López-Alba, L. Felipe-Sesé, F.A. Díaz, Full-field modal analysis during base motion excitation using high-speed 3D digital image correlation, Meas. Sci. Technol. 28 (2017), 105402, https://doi.org/10.1088/1361-6501/aa7d87.
[5] P.L. Reu, D.P. Rohe, L.D. Jacobs, Comparison of DIC and LDV for practical vibration and modal measurements, Mech. Syst. Signal Process. 86 (2017) 2–16, https://doi.org/10.1016/j.ymssp.2016.02.006.
[6] F. Trebuňa, M. Hagara, Experimental modal analysis performed by high-speed digital image correlation system, Measurement. 50 (2014) 78–85, https://doi.org/10.1016/j.measurement.2013.12.038.
[7] W. Wang, J.E. Mottershead, T. Siebert, A. Pipino, Frequency response functions of shape features from full-field vibration measurements using digital image correlation, Mech. Syst. Signal Process. 28 (2012) 333–347, https://doi.org/10.1016/j.ymssp.2011.11.023.
[8] M. Takeda, K. Mutoh, Fourier transform profilometry for the automatic measurement of 3-D object shapes, Appl. Opt. 22 (1983) 3977, https://doi.org/10.1364/AO.22.003977.
[9] C. Zuo, S. Feng, L. Huang, T. Tao, W. Yin, Q. Chen, Phase shifting algorithms for fringe projection profilometry: A review, Opt. Lasers Eng. 109 (2018) 23–59, https://doi.org/10.1016/j.optlaseng.2018.04.019.
[10] D. Feng, M.Q. Feng, Computer vision for SHM of civil infrastructure: From dynamic response measurement to damage detection – A review, Eng. Struct. 156 (2018) 105–117, https://doi.org/10.1016/j.engstruct.2017.11.018.
[11] S. Zhang, High-speed 3D shape measurement with structured light methods: A review, Opt. Lasers Eng. 106 (2018) 119–131, https://doi.org/10.1016/j.optlaseng.2018.02.017.
[12] S.S. Gorthi, P. Rastogi, Fringe projection techniques: Whither we are? Opt. Lasers Eng. 48 (2010) 133–140, https://doi.org/10.1016/j.optlaseng.2009.09.001.
[13] L. Felipe-Sesé, P. Siegmann, F.A. Díaz, E.A. Patterson, Simultaneous in-and-out-of-plane displacement measurements using fringe projection and digital image correlation, Opt. Lasers Eng. 52 (2014) 66–74, https://doi.org/10.1016/j.optlaseng.2013.07.025.
[14] L. Felipe-Sesé, E. López-Alba, F.A. Díaz, Full-field 3D displacement and strain analysis during low energy impact tests employing a single-camera system, Thin-Walled Struct. 148 (2020), https://doi.org/10.1016/j.tws.2019.106584.
[15] L. Felipe-Sesé, F.A. Díaz, Damage methodology approach on a composite panel based on a combination of Fringe Projection and 2D Digital Image Correlation, Mech. Syst. Signal Process. 101 (2018) 467–479, https://doi.org/10.1016/j.ymssp.2017.09.002.
[16] Á.J. Molina-Viedma, L. Felipe-Sesé, E. López-Alba, F.A. Díaz, Comparative of conventional and alternative Digital Image Correlation techniques for 3D modal characterisation, Meas. J. Int. Meas. Confed. 151 (2020), https://doi.org/10.1016/j.measurement.2019.107101.
[17] N.A. Hoult, W. Andy Take, C. Lee, M. Dutton, Experimental accuracy of two dimensional strain measurements using Digital Image Correlation, Eng. Struct. 46 (2013) 718–726, https://doi.org/10.1016/j.engstruct.2012.08.018.
[18] Y. Barranger, P. Doumalin, J.C. Dupré, A. Germaneau, Digital image correlation accuracy: Influence of kind of speckle and recording setup, EPJ Web Conf. 6 (2010) 31002.
[19] H. Nguyen, J. Liang, Y. Wang, Z. Wang, Accuracy assessment of fringe projection profilometry and digital image correlation techniques for three-dimensional shape measurements, JPhys Photonics. 3 (2021), https://doi.org/10.1088/2515-7647/abcbe4.
[20] L. Felipe-Sesé, Á.J. Molina-Viedma, E. López-Alba, F.A. Díaz, RGB colour encoding improvement for three-dimensional shapes and displacement measurement using the integration of fringe projection and digital image correlation, Sensors (Switzerland). 18 (2018), https://doi.org/10.3390/s18093130.
[21] N. Wadhwa, M. Rubinstein, F. Durand, W.T. Freeman, Phase-based video motion processing, ACM Trans. Graph. 32 (2013) 1, https://doi.org/10.1145/2461912.2461966.
[22] J.G. Chen, N. Wadhwa, Y.-J. Cha, F. Durand, W.T. Freeman, O. Buyukozturk, Modal identification of simple structures with high-speed video using motion magnification, J. Sound Vib. 345 (2015) 58–71, https://doi.org/10.1016/j.jsv.2015.01.024.
[23] M. Rubinstein, E. Shih, J. Guttag, F. Durand, W. Freeman, E. Video, H. Wu, Video Magnification, (2015). http://people.csail.mit.edu/mrub/vidmag/ (accessed September 7, 2021).
[24] A.J. Molina-Viedma, L. Felipe-Sesé, E. López-Alba, F. Díaz, High frequency mode shapes characterisation using Digital Image Correlation and phase-based motion magnification, Mech. Syst. Signal Process. 102 (2018) 245–261, https://doi.org/10.1016/j.ymssp.2017.09.019.
[25] A.J. Molina-Viedma, L. Felipe-Sesé, E. López-Alba, F.A. Díaz, 3D mode shapes characterisation using phase-based motion magnification in large structures using stereoscopic DIC, Mech. Syst. Signal Process. 108 (2018) 140–155, https://doi.org/10.1016/j.ymssp.2018.02.006.
[26] Á.J. Molina-Viedma, E. López-Alba, L. Felipe-Sesé, F.A. Díaz, Operational Deflection Shape Extraction from Broadband Events of an Aircraft Component Using 3D-DIC in Magnified Images, Shock Vib. 2019 (2019), https://doi.org/10.1155/2019/4039862.
[27] Y.E. Harmanci, U. Gülan, M. Holzner, E. Chatzi, A novel approach for 3D-structural identification through video recording: Magnified tracking, Sensors (Switzerland). 19 (2019) 1–16, https://doi.org/10.3390/s19051229.
[28] M. Civera, L. Zanotti Fragonara, C. Surace, An experimental study of the feasibility of phase-based video magnification for damage detection and localisation in operational deflection shapes, Strain. 56 (2020) 1–19, https://doi.org/10.1111/str.12336.
[29] M. Eitner, B. Miller, J. Sirohi, C. Tinney, Effect of broad-band phase-based motion magnification on modal parameter estimation, Mech. Syst. Signal Process. 146 (2020), 106995, https://doi.org/10.1016/j.ymssp.2020.106995.
[30] Y. Yang, C. Dorn, C. Farrar, D. Mascareñas, Blind, simultaneous identification of full-field vibration modes and large rigid-body motion of output-only structures from digital video measurements, Eng. Struct. 207 (2020), 110183, https://doi.org/10.1016/j.engstruct.2020.110183.
[31] D.P. Rohe, P.L. Reu, Experimental Modal Analysis Using Phase Quantities from Phase-Based Motion Processing and Motion Magnification, Exp. Tech. 45 (2021) 297–312, https://doi.org/10.1007/s40799-020-00392-7.
[32] E.P. Simoncelli, W.T. Freeman, The steerable pyramid: a flexible architecture for multi-scale derivative computation, in: Proc. Int. Conf. Image Process., 1995: pp. 444–447. 10.1109/ICIP.1995.537667.
[33] D.J. Fleet, A.D. Jepson, Computation of component image velocity from local phase information, Int. J. Comput. Vis. 5 (1990) 77–104, https://doi.org/10.1007/BF00056772.
[34] T. Gautama, M.a., a Van Hulle, A phase-based approach to the estimation of the optical flow field using spatial filtering, IEEE Trans. Neural Networks. 13 (2002) 1127–1136, https://doi.org/10.1109/TNN.2002.1031944.
[35] M. Sutton, W. Wolters, W. Peters, W. Ranson, S. McNeill, Determination of displacements using an improved digital correlation method, Image Vis. Comput. 1 (1983) 133–139, https://doi.org/10.1016/0262-8856(83)90064-1.
[36] P. Siegmann, V. Álvarez-Fernández, F. Díaz-Garrido, E.A. Patterson, A simultaneous in- and out-of-plane displacement measurement method, Opt. Lett. 36 (2011) 10, https://doi.org/10.1364/OL.36.000010.
[37] C. Mares, B. Barrientos, A. Blanco, Measurement of transient deformation by color encoding, Opt. Express. 19 (2011), https://doi.org/10.1364/OE.19.025712.
[38] B. Pan, K. Qian, H. Xie, A. Asundi, Two-dimensional digital image correlation for in-plane displacement and strain measurement : a review, Meas. Sci. Technol. 20 (2009) 1–17, https://doi.org/10.1088/0957-0233/20/6/062001.
[39] L. Felipe-Sesé, P. Siegmann, F.A. Díaz, E.A. Patterson, Integrating fringe projection and digital image correlation for high-quality measurements of shape changes, Opt. Eng. 53 (2014), 044106, https://doi.org/10.1117/1.OE.53.4.044106.
[40] P. Siegmann, L. Felipe-Sese, F. Diaz-Garrido, Improved 3D displacement measurements method and calibration of a combined fringe projection and 2D-DIC system, Opt. Lasers Eng. 88 (2017) 255–264, https://doi.org/10.1016/j.optlaseng.2016.08.014.
[41] D. Ghiglia, M. Pritt, Two-dimensional phase unwrapping: theory, algorithms, and software, 1998. 10.1177/004057368303900411.
[42] L. Felipe-Sesé, Á.J. Molina-Viedma, E. López-Alba, F.A. Díaz, FP+DIC for low-cost 3D full-field experimental modal analysis in industrial components, Mech. Syst.

Signal Process. 128 (2019) 329–339, https://doi.org/10.1016/j.ymssp.2019.04.004.

JCR YEAR

2021

MEASUREMENT

ISSN

0263-2241

EISSN

1873-412X

JCR ABBREVIATION

MEASUREMENT

ISO ABBREVIATION

Measurement

Journal information

EDITION

Science Citation Index Expanded (SCIE)

CATEGORY

INSTRUMENTS & INSTRUMENTATION - SCIE

ENGINEERING, MULTIDISCIPLINARY - SCIE

LANGUAGES	REGION	1ST ELECTRONIC JCR YEAR
English	ENGLAND	2002

Publisher information

PUBLISHER	ADDRESS	PUBLICATION FREQUENCY
ELSEVIER SCI LTD	THE BOULEVARD, LANGFORD LANE, KIDLINGTON, OXFORD OX5 1GB, OXON, ENGLAND	8 issues/year

Journal's performance

Journal Impact Factor

The Journal Impact Factor (JIF) is a journal-level metric calculated from data indexed in the Web of Science Core Collection. It should be used with careful attention to the many factors that influence citation rates, such as the volume of publication and citations characteristics of the subject area and type of journal. The Journal Impact Factor can complement expert opinion and informed peer review. In the case of academic evaluation for tenure, it is inappropriate to use a journal-level metric as a proxy measure for individual researchers, institutions, or articles. Learn more

2021 JOURNAL IMPACT FACTOR

5.131

View calculation

JOURNAL IMPACT FACTOR WITHOUT SELF CITATIONS

4.170

View calculation

Journal Impact Factor contributing items

Export

Journal Impact Factor Trend 2021

Export

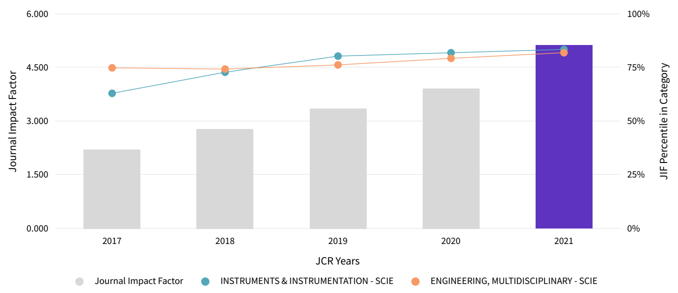

View all years

Citable items (2,260) | Citing Sources (1,747)

TITLE	CITATION COUNT
A review of failure modes, condition monitoring and fault diagnosis methods fo…	81
Identifying pneumonia in chest X-rays: A deep learning approach	60
Machinery fault diagnosis with imbalanced data using deep generative adversarial…	57
An adaptive deep transfer learning method for bearing fault diagnosis	51
Optimal bilateral filter and Convolutional Neural Network based denoising method o…	49
Research and application of improved adaptive MOMEDA fault diagnosis method	44
Latest developments in gear defect diagnosis and prognosis: A review	42
Rolling bearing fault diagnosis using generalized refined composite multiscale…	41
A novel gas turbine fault diagnosis method based on transfer learning with CNN	40
Investigation of progressive tool wear for determining of optimized machining…	39

Journal Citation Indicator (JCI)

Export

1.52

The Journal Citation Indicator (JCI) is the average Category Normalized Citation Impact (CNCI) of citable items (articles & reviews) published by a journal over a recent three year period. The average JCI in a category is 1. Journals with a JCI of 1.5 have 50% more citation impact than the average in that category. It may be used alongside other metrics to help you evaluate journals. Learn more

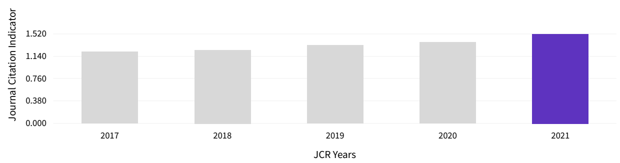

31,214

The total number of times that a journal has been cited by all journals included in the database in the JCR year. Citations to journals listed in JCR are compiled annually from the JCR years combined database, regardless of which JCR edition lists the journal.

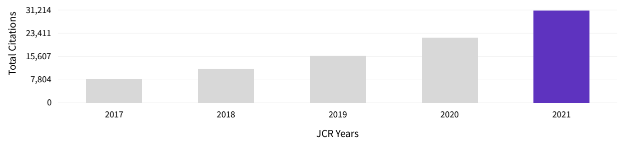

View all years

Citation distribution

Export

The Citation Distribution shows the frequency with which items published in the year or two years prior were cited in the JCR data year (i.e., the component of the calculation of the JIF). The graph has similar functionality as the JIF Trend graph, including hover-over data descriptions for each data point, and an interactive legend where each data element's legend can be used as a toggle. You can view Articles, Reviews, or Non-Citable (other) items to the JIF numerator. Learn more

ARTICLE CITATION MEDIAN

3

REVIEW CITATION MEDIAN

4

UNLINKED CITATIONS

306

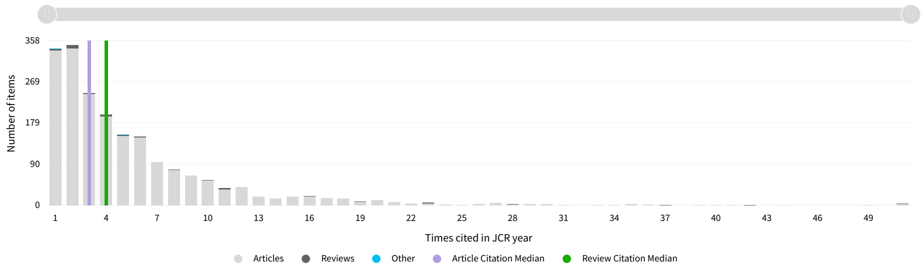

TIMES CITED

0

ARTICLES

275

REVIEWS

2

OTHER

14

Open Access (OA)

Export

The data included in this tile summarizes the items published in the journal in the JCR data year and in the previous two years. For example, in the 2020 JCR data, released in June 2021, the Open Access (OA) data show the publication model (Gold OA or subscription) of materials published in 2018, 2019 and 2020, and citations in 2020 to these items. This three-year set of published items is used to provide descriptive analysis of the content and community of the journal. Learn more

Items

TOTAL CITABLE	% OF CITABLE OA
4,044	4.10%

CITABLE

GOLD OPEN ACCESS
166 / 4.08%

SUBSCRIPTION AND FREE TO READ
3,878 / 95.31%

NON-CITABLE

OTHER (NON CITABLE ITEMS)
25 / 0.61%

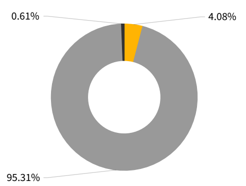

Citations*

TOTAL CITABLE	% OF CITABLE OA
14,105	2.13%

CITABLE

GOLD OPEN ACCESS
301 / 2.08%

SUBSCRIPTION AND FREE TO READ
13,804 / 95.30%

NON-CITABLE

OTHER (NON CITABLE ITEMS)
6 / 0.04%

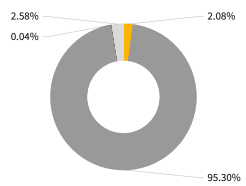

UNLINKED CITATIONS

374 / 2.58%

*Citations in 2021 to items published in [2019 - 2021]

Rank by Journal Impact Factor

Journals within a category are sorted in descending order by Journal Impact Factor (JIF) resulting in the Category Ranking below. A separate rank is shown for each category in which the journal is listed in JCR. Data for the most recent year is presented at the top of the list, with other years shown in reverse chronological order. Learn more

EDITION

Science Citation Index Expanded (SCIE)

CATEGORY

ENGINEERING, MULTIDISCIPLINARY

17/92

JCR YEAR	JIF RANK	JIF QUARTILE	JIF PERCENTILE
2021	17/92	Q1	82.07
2020	19/90	Q1	79.44
2019	22/91	Q1	76.37
2018	23/88	Q2	74.43
2017	22/86	Q2	75.00

EDITION

Science Citation Index Expanded (SCIE)

CATEGORY

INSTRUMENTS & INSTRUMENTATION

11/64

JCR YEAR	JIF RANK	JIF QUARTILE	JIF PERCENTILE
2021	11/64	Q1	83.59
2020	12/64	Q1	82.03
2019	13/64	Q1	80.47
2018	17/61	Q2	72.95
2017	23/61	Q2	63.11

Rank by Journal Citation Indicator (JCI)

Journals within a category are sorted in descending order by Journal Citation Indicator (JCI) resulting in the Category Ranking below. A separate rank is shown for each category in which the journal is listed in JCR. Data for the most recent year is presented at the top of the list, with other years shown in reverse chronological order. Learn more

CATEGORY

ENGINEERING, MULTIDISCIPLINARY

17/175

JCR YEAR	JCI RANK	JCI QUARTILE	JCI PERCENTILE
2021	17/175	Q1	90.57
2020	20/170	Q1	88.53
2019	23/169	Q1	86.69
2018	25/168	Q1	85.42
2017	27/168	Q1	84.23

CATEGORY

INSTRUMENTS & INSTRUMENTATION

6/76

JCR YEAR	JCI RANK	JCI QUARTILE	JCI PERCENTILE
2021	6/76	Q1	92.76
2020	7/72	Q1	90.97
2019	7/72	Q1	90.97
2018	9/70	Q1	87.86
2017	8/69	Q1	89.13